Theoretical study of doped $Tl_2Mn_2O_7$ and $Tl_2Mn_2O_7$ under pressure

Molly De Raychaudhury,[1] T. Saha-Dasgupta,[1] and D. D. Sarma[2,3,*]
[1]*S.N. Bose National Centre for Basic Sciences, Kolkata 700098, India*
[2]*Indian Association for the Cultivation of Science, Jadavpur, Kolkata 700032, India*
[3]*Solid State and Structural Chemistry Unit, Indian Institute of Science, Bangalore-560012, India*
(Received 10 October 2006; revised manuscript received 28 November 2006; published 31 January 2007)

Using first-principles density-functional-based calculations, we study the effect of doping and pressure on the manganese-based pyrochlore compound, $Tl_2Mn_2O_7$, which exhibits colossal magnetoresistive behavior. The theoretical study is motivated by the counterintuitive experimental observation of suppression of the ferromagnetic transition temperature upon application of pressure and its enhancement upon substitution of Mn by a moderate amount of nonmagnetic Sb ion. We also attempt to resolve the issue related to crystal structure changes that may occur upon application of pressure.

DOI: 10.1103/PhysRevB.75.014443 PACS number(s): 75.47.Gk

I. INTRODUCTION

Manganese-based pyrochlore compounds, such as $Tl_2Mn_2O_7$, form an interesting class of compounds which despite having similar colossal magnetoresistive (CMR) effects exhibit markedly different features compared to that of manganites. In contrast to manganites, these compounds are not mixed valent, do not have any appreciable Jahn-Teller distortion,[1] and seemingly show metallic behavior[2] both below and above the magnetic transition temperature T_c ($\approx$140 K). Concerning the metallic behavior above T_c though, it is not totally clear whether it is a good metal or more like a bad metal or an insulatorlike compound which arises due to difficulties related to sample preparation and defects present in the paramagnetic phase. Though the original data by Shimakawa *et al.*[2] suggests the metallic behavior above T_c, the optical conductivity data[3] and photoemission and x-ray absorption near edge spectroscopy[4] point towards an insulatorlike behavior in the paramagnetic regions. These nonmanganitelike features rule out the generally applicable double-exchange mechanism or polaronic mechanism as the driving mechanism of ferromagnetism in this class of compound and remained a mystery for quite some time. In absence of a double-exchange mechanism, a strong contestant for the driving mechanism is the Mn-O-Mn-mediated superexchange mechanism, particularly since Mn-O-Mn forms an angle[5] of 133°, significantly smaller than 180°. This is, however, contradicted by the experimental findings that the ferromagnetic T_c gets suppressed by application of pressure[6] and gets enhanced by a moderate amount of the introduction of nonmagnetic ions like Sb in place of Mn.[7] Employing an *N*th-order muffin-tin-orbital- (MTO-) based NMTO-downfolding technique,[8] we have recently established[9] that the driving mechanism of ferromagnetism in this class of compounds is neither superexchange or double exchange nor any exotic mechanism with nearest-neighbor-(NN) antiferromagnetic (AFM) coupling dominated by long-ranged ferromagnetic (FM) interactions,[10] but a kinetic-energy-assisted mechanism similar to that of double-perovskite compounds like Sr_2FeMoO_6, Sr_2FeReO_6,[11,12] and Mn-doped GaAs.[13]

In the present paper, we give a detailed account of the doping effect and the pressure effect from the electronic structure point of view, which lends further support to the existence of the proposed kinetic energy driven mechanism in these compounds. While the changes that happen in the crystal structure upon doping are clear, the situation is rather ambiguous in the case of the application of pressure. The initial measurement hinted at a decrease in Mn-O-Mn bond angle[6,14] along with compression of Mn-O bond length. However, a subsequent measurement[15] indicated an increase in the Mn-O-Mn bond angle which was used in terms of a superexchange mechanism to explain the decrease in T_c. In view of these conflicting claims, we also take the opportunity to theoretically address the effect of pressure on the structure of $Tl_2Mn_2O_7$ and its implication to magnetism by detailed electronic structure calculations together with structural relaxations under pressure.

The rest of the paper is organized in the following way. Section II deals with various methodologies that have been employed to compute the crystallographic structure (in the case of $Tl_2Mn_2O_7$ under pressure) and to compute and analyze the subsequent electronic structure of $Tl_2Mn_2O_7$ under doping and pressure. In Sec. III, we present our results. This section is divided into several subsections. In Sec. III A, the electronic structure of pristine $Tl_2Mn_2O_7$ is presented and the proposed kinetic-energy-driven mechanism is introduced as a reference, which will form the basis of discussion in the following. Section III B is devoted to $Tl_2Mn_2O_7$ under pressure, while Sec. III C is devoted to Sb-doped $Tl_2Mn_2O_7$. Finally, we conclude the paper with a summary presented in Sec. IV.

II. METHODOLOGY

We have investigated the electronic structure of pure $Tl_2Mn_2O_7$, $Tl_2Mn_{2-x}Sb_xO_7$, and $Tl_2Mn_2O_7$ under pressure by the tight-binding linear muffin-tin orbital[16] (LMTO) method, computed within the framework of the local spin density approximation (LSDA) of the density functional theory (DFT). The basis set employed consisted of Tl 6*s*, 6*p*, and 5*d* states, Mn 4*s*, 4*p*, and 3*d* states, and O 2*s* and 2*p* states. Three different classes of empty spheres were used to fill up the space. The self-consistent calculations were performed on a Brillouin zone (BZ) mesh of $12\times12\times12$.

The computed band structures were analyzed and interpreted in terms of the NMTO-downfolding technique.[8] The NMTO technique, introduced and implemented in recent years, goes beyond the scope of standard linear MTO (LMTO) technique by defining an energetically accurate basis with consistent description throughout the space involving both the MT spheres and the interstitial. An important feature of this technique is the energy-selective downfolding procedure where one integrates out degrees of freedom and keeps only few degrees of freedom active to define a few-orbital, low-energy Hamiltonian. The effective NMTO's defining such Hamiltonian serve as a Wannier or Wannier-like function corresponding to the selected low-energy bands.

For the calculation of the exchange interaction strengths J, a supercell involving a 16 Mn atoms was constructed, which amounts to enlarging the original unit cell by 4 times. This was achieved by replacing the original face-centered-cubic (fcc) lattice by the simple cubic lattice with 4 times as many atoms as that in fcc. The basic structural unit of Mn sublattices is the Mn_4 tetrahedra which share corners to form an infinite three-dimensional (3D) lattice. We calculated the LSDA total energies by considering different magnetic configurations of this sublattice. In total, six spin configurations have been chosen. One of the six configurations was FM and the other five were AFM. The details of the spin configurations chosen are as given in Table I in Ref. 9. The total energies are then mapped on to an effective Heisenberg Hamiltonian formed by the Mn^{+4} spins. The Hamiltonian considered until the third-nearest-neighbor (3NN) interactions is

$$H = J_1 \sum_{nn} S_i \cdot S_j + J_2 \sum_{2nn} S_i \cdot S_j + J_3 \sum_{3nn} S_i \cdot S_j, \qquad (1)$$

where S_i denotes the spin-3/2 operator corresponding to the Mn^{+4} spins at site i and J_1, J_2, and J_3 denote the NN, 2NN, and 3NN magnetic exchange interaction strengths. Since we have restricted ourselves to only five AFM configurations among many possible AFM configurations, we computed seven different estimates of these J's along with their standard deviations employing set of three energy differences chosen out of total five different energy differences. This limitation can be overcome by taking as many AFM spin configurations as practically possible. The mean-field estimate of T_c is given by

$$T_c^{mf} = \frac{S(S+1)}{3k_B} J_0, \qquad (2)$$

where J_0 is the net effective magnetic exchange interaction given by

$$J_0 = z_1 J_1 + z_2 J_2 + z_3 J_3 \qquad (3)$$

and $S = \frac{3}{2}$. Here k_B is the Boltzman constant and z_1, z_2, and z_3 are the number of NN, 2NN, and 3NN Mn pairs. For undoped $Tl_2Mn_2O_7$, $z_1 = 6$, $z_2 = 12$, and $z_3 = 12$. However, these numbers change in the case of doped calculations where some of the Mn atoms get replaced by nonmagnetic Sb ions and therefore do not contribute in the calculation of the magnetic energy. The application of mean-field theory is naturally expected to overestimate the T_c. Use of Monte Carlo simulation[17] or Green function method[18] can give better estimates and agreements with experimentally measured values. One needs to keep this in mind when comparisons are being made with the measured T_c in the following sections.

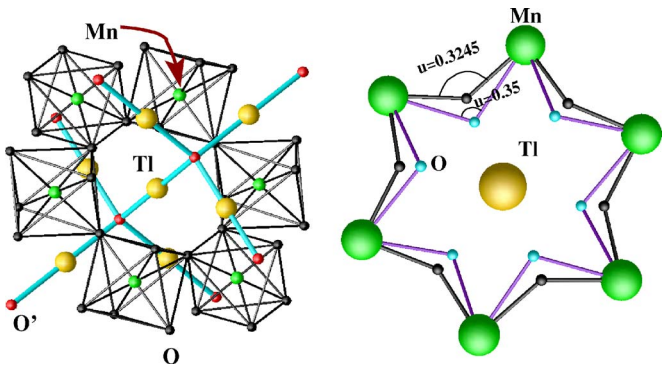

FIG. 1. (Color online) Left panel: The $Tl_2Mn_2O_7$ structure consisting of the ring formed by MnO_6 octahedra with Tl-O′ rods passing through the holes of the rings. Right panel: Backbone of the structure realized by the ring like structure formed by the Mn-O-Mn network (the Tl-O′ rod network is not shown for clarity). Gold, green and black or cyan spheres denote the Tl, Mn and O atoms. Black and cyan spheres correspond to oxygen (O) atoms with two different oxygen (O) position parameter u.

$Tl_2Mn_2O_7$ occurs in a cubic, face-centered lattice with Fd-3m space group and two formula units in the cell.[5] There are two types of oxygens, O′ and O. While O oxygens provide the octahedral surrounding of the Mn atom which corner share to give rise to a geometry of a closed ring or cage, O′ atoms form nearest-neighbor bonds with Tl giving rise to a Tl_2O' complex running through the cagelike geometry as shown in left panel of Fig. 1. The structural parameters for the pristine $Tl_2Mn_2O_7$ and Sb-doped $Tl_2Mn_2O_7$ have been taken as the experimentally determined structure published in the literature.[7,19] However, as mentioned already, the structural information for $Tl_2Mn_2O_7$ under pressure is somewhat controversial which calls for structural optimization. For this purpose, we have adopted the pseudopotential method[20] as implemented in the VASP[21] code. We have employed the pseudopotentials generated by the projector-augmented-wave[22] (PAW) method. Wave functions have been expanded in terms of plane waves with a cutoff energy of 400 eV. A k mesh of $6\times6\times6$ was employed to perform the self-consistent calculations. In $Tl_2Mn_2O_7$, Tl, Mn, O′ and O atoms occupy the Wyckoff positions 16d, 16c, 8b, and 48f, respectively. Among these only the positions given by 48f contain the internal parameter u. This parameter u defines the ∠Mn-O-Mn (see right panel of Fig. 1). As u increases, the ∠Mn-O-Mn decreases and vice versa. When pressure is applied, it needs to be investigated whether the u parameter also varies along with the reduction in the bond lengths. If at all it changes, it has to be ascertained in what way it does so. In our calculation, the O position is relaxed by varying u, in order to find out the variation of total energy with angle formed between Mn, O, and Mn atoms. In order to obtain the theoretical ground state and cohesive properties and estimate the pressure, a Murnaghan[23] equation of state

has been employed to fit the LSDA total energies. The Murnaghan equation of state is given by

$$E(V) = E_0 + \frac{B_0 V}{B_0'}\left[\frac{(V_0/V)^{B_0'}}{B_0' - 1} + 1\right] - \frac{B_0 V_0}{B_0' - 1}, \quad (4)$$

where V_0 is the equilibrium volume and B_0 is the bulk modulus and is given by $B_0 = -V(\delta P/\delta V)_T$ evaluated at volume V_0. B_0' is the pressure derivative of B_0 also evaluated at volume V_0. B_0' provides a measure of stiffness of the material upon increasing pressure. Typical values for the parameter B_0' are between 4 and 7. The pressure P corresponding to volume V occupied by a cell of a particular lattice parameter is given by

$$P(V) = \frac{B_0}{B_0'}[(V_0/V)^{B_0'} - 1]. \quad (5)$$

III. RESULTS

A. FM electronic structure of pristine $Tl_2Mn_2O_7$ and the underlying mechanism

The LSDA electronic structure of ferromagnetically ordered $Tl_2Mn_2O_7$, computed with the tight-binding (TB) LMTO method is shown in Fig. 2. This figure shows both the band structure and the orbital projected density of states (DOS). Consistent with the nominal valence of O^{2-} and Mn^{4+}, oxygen-dominated states are totally occupied, while the crystal-field-split Mn t_{2g} states are occupied in the majority-spin channel and close to empty in the minority-spin channel. Mn e_g states consistent with the $3d^3$ configuration of Mn remain empty in both the spin channels. Tl bands, consistent with Tl^{3+} nominal valence, also remain almost empty. However, interestingly in the majority-spin channel, the Tl 6s state mixed with O′ 2p states overlaps with the Mn e_g manifold spanning an energy range of about 2–4 eV,[24] while in the minority-spin channel, they overlap with nearly empty Mn t_{2g}–dominated states, which gives rise to a highly dispersive band in the bottom of this manifold, crossing the Fermi level E_F, as seen in the lower, left panel of Fig. 2. This hints at a large spin splitting at the Tl site. This is unusual in the sense that one would normally expect Tl to be essentially nonmagnetic with tiny spin splitting. This unusual feature plays the key role in providing the understanding of the driving mechanism of ferromagnetism in $Tl_2Mn_2O_7$. This has been explained in detail in Ref. 9. As has been shown in Ref. 9, the unhybridized effective Tl-O′ level is positioned in between the spin-split Mn t_{2g} states, and on turning on the hybridization, it induces a renormalized spin splitting within the Tl-O′ level which is directed in an opposite way compared to the spin splitting at the Mn site. This happens due to a pushing up of the Tl-O′ spin-up state and a pushing down of the Tl-O′ spin-down states, driven by coupling with the Mn t_{2g} states of the same symmetry. The energy gain contributed by this hybridization-induced negative spin polarization of the otherwise nonmagnetic element is the central concept in this novel mechanism. This mechanism ensures a specific spin orientation between the localized Mn t_{2g} spins and the mobile carrier formed by the hybridized renormalized state, which in turn aligns the spins in Mn sublattice. This is a general mechanism and is found to be operative in the case of a number of compounds like Sr_2FeMoO_6, Sr_2FeReO_6,[11,12] Mn-doped GaAs,[13] $CuCr_2S_4$,[25] etc.

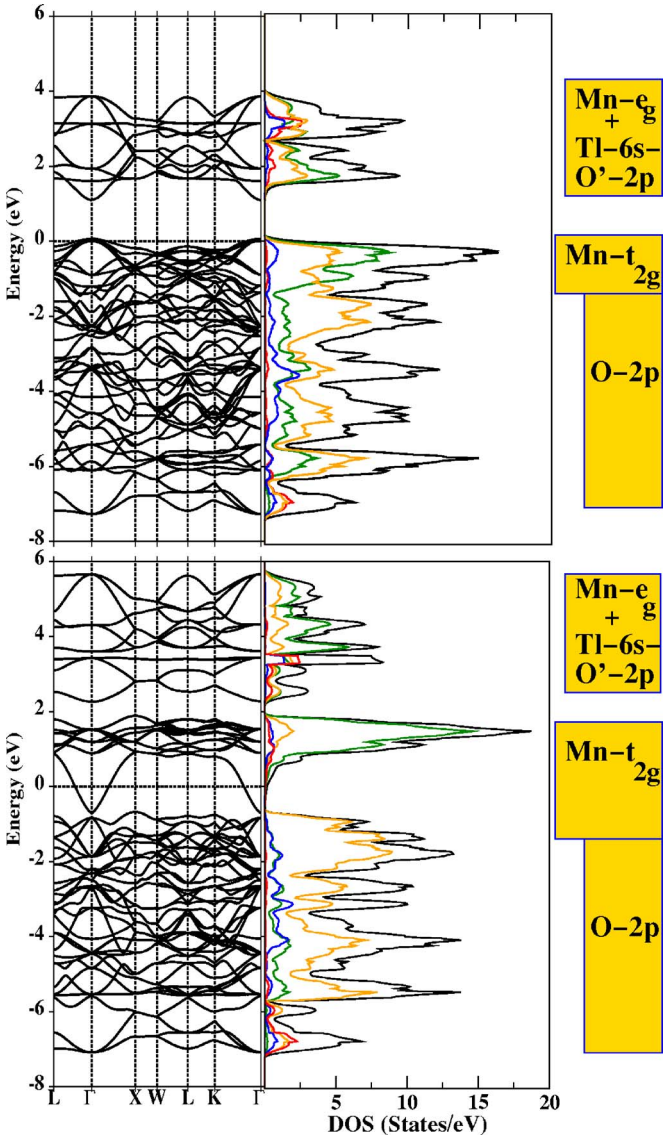

FIG. 2. (Color online) Left panels show the spin-polarized band structure computed within the LSDA for $Tl_2Mn_2O_7$. The zero of the energy is set at the LSDA Fermi energy E_F. Right panels give the spin-polarized total (black), Tl 6s (red), Mn 3d (green), O 2p (orange), and O′ 2p (blue) density of states. Upper and lower figures correspond to the majority- and minority-spin contributions, respectively, in both the panels. Bars on the right signify the energy range for which various characters dominate.

In the following subsections, we will present a detail account of the changes in the electronic structure and the variation in T_c of $Tl_2Mn_2O_7$ with doping and under pressure. We will argue that the counterintuitive variation in T_c has its origin in the modified electronic structure and follows naturally from the framework of the proposed hybridization-

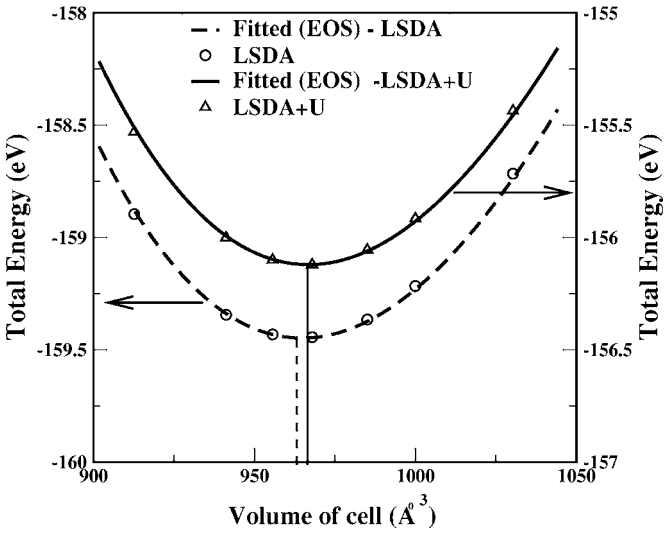

FIG. 3. Total energy vs volume of the unit cell calculations within the LSDA and LSDA+U. The symbols denote the DFT total energies, and the solid and dashed lines depict the total energies obtained from fitting with Murnaghan (Ref. 23) equation of state (EOS).

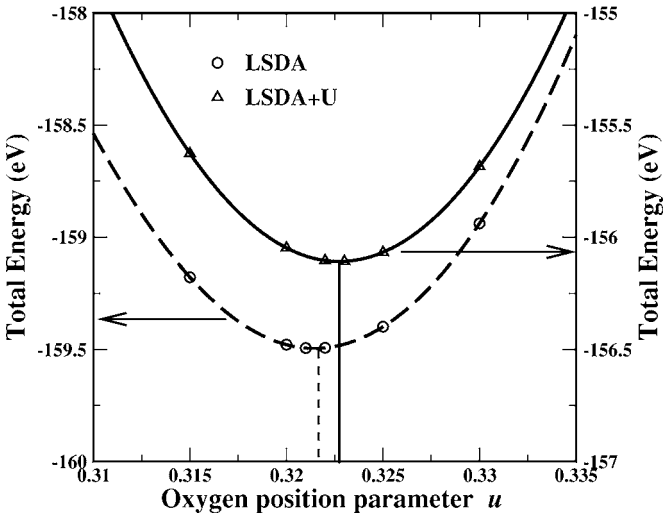

FIG. 4. Relaxation of the oxygen (O) position parameter u at ambient condition within the LSDA and LSDA+U in $Tl_2Mn_2O_7$. The symbols are the DFT total energies, and the solid and dashed lines are cubic splines interpolated.

induced mechanism of ferromagnetism as was established in Ref. 9 and reviewed above.

B. $Tl_2Mn_2O_7$ under pressure

As explained before, to investigate $Tl_2Mn_2O_7$ under pressure one needs to first settle the issues related to crystal structure. To be precise, does applied pressure increase or decrease or not alter the ∠Mn-O-Mn? For this purpose, we have carried out a series of structural optimization calculations with the pseudopotential method.[20] At first the cohesive properties were calculated within the LSDA. Following the recent claim[26] that application of on-site U can also influence the cohesive properties of transition metal oxides, we have repeated our calculations also with LSDA+U functionals.

The LSDA total energy vs volume calculation, shown in Fig. 3, has a minimum corresponding to lattice constant of 9.881 Å. Considering that the experimental value of the lattice constant is 9.892 Å, this gives a deviation of about 0.1%, which is within the limit of the LSDA overbinding. The value of the bulk modulus, obtained by fitting the total energy versus volume curve with the Murnagahan equation of state,[23] is 230.6 GPa, which is of the same order as the experimentally measured value of ≈200 GPa in $Tl_{1.8}Cd_{0.2}Mn_2O_7$.[15] B_0' is +4.84, much higher than that in Cd-doped $Tl_2Mn_2O_7$ but within the expected limit. Applying an on-site Coulomb interaction of $U=2$ eV and $J=0.7$ eV on the Mn site leads to a slightly better agreement with the experimental values. The lattice parameter changes to 9.888 Å; B_0 and B_0' remain unaltered. In view of the slightly improved results of LSDA+U, we have used the B_0 and B_0' as estimated by LSDA+U calculations to compute the pressure as given by Eq. (5).

Until now we have considered the experimental ∠Mn-O-Mn as the one for the theoretical ground state. One needs to relax this angle in order to obtain the true theoretically predicted ground state. The coordinate of O atom in the basis is given by $(u, 0.125, 0.125)$. The u parameter will push the O atom in or out depending on its value, thereby changing the angle formed between Mn, O, and Mn atoms. The u parameter is relaxed in the subsequent calculations, and the LSDA (for 9.881 Å) and LSDA+U total energies (for 9.888 Å) are computed varying the u parameter. The minimum in the E vs u curve (see Fig. 4) is obtained for $u=0.3214$ and 0.3227, respectively. The ∠Mn-O-Mn in the ground state obtained within the LSDA and LSDA+U framework are given in Table I along with the corresponding

TABLE I. Calculated ground-state structural parameters of $Tl_2Mn_2O_7$ within the LSDA and LSDA+U compared with the experimental (Ref. 5) data at ambient condition.

	LDA	LSDA+U	Expt.
a (Å)	9.881	9.888	9.892
u	0.3214	0.3227	0.3254
Mn-O (Å)	1.886	1.890	1.901
∠Mn-O-Mn (deg)	136.01	135.29	133.8
B_0 (GPa)	230.6	230.7	
B_0'	+4.84	+4.85	

TABLE II. Structural parameters obtained within the LSDA+U at ambient and two different pressures upon relaxation of the oxygen (O) position parameter u in $Tl_2Mn_2O_7$.

	Ambient	3.04 GPa	16.28 GPa
u	0.3227	0.3230	0.3234
Mn-O (Å)	1.890	1.883	1.854
∠Mn-O-Mn (deg)	135.29	135.18	134.90

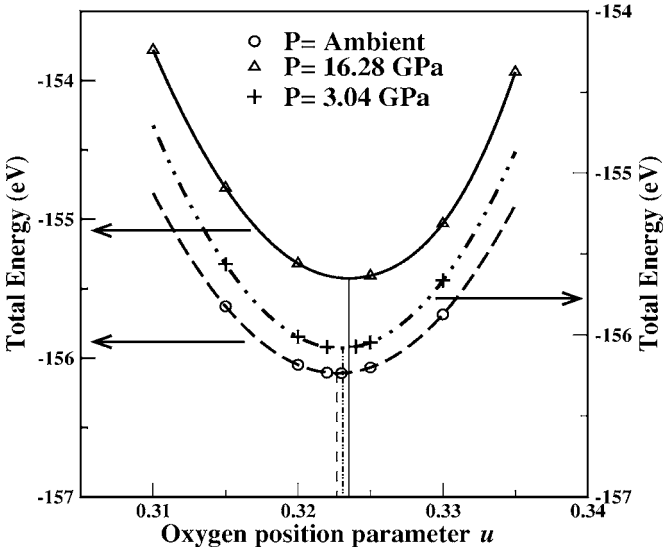

FIG. 5. Total energy vs u, i.e., relaxation of the oxygen (O) position parameter u at ambient condition and under pressure of 3.04 and 16.28 GPa within the LSDA+U in $Tl_2Mn_2O_7$. The symbols are the DFT total energies, and the solid, dashed, and dash-dotted lines are cubic splines interpolated.

experimental values. Slightly better results are obtained for the LSDA+U calculations, a trend already observed in calculations of equilibrium lattice constant. The results match with experimental values up to the second decimal point for u and within 1.5° for the Mn-O-Mn angle.

Having established the ground state, in the next step we relax the O position for lattice parameters a=9.846 and 9.69 Å (LSDA+U) which amounts to applying a pressure of 3.04 GPa and 16.28 GPa. This will clarify whether the Mn-O-Mn angle also changes with the decrease in the interatomic distances. The minima obtained from the total energy versus u plots, as shown in Fig. 5, are listed in Table II. We find that on application of pressure, the ∠Mn-O-Mn reduces *insignificantly*, by about 0.1° and 0.4° for a pressure of 3.04 GPa and 16.28 GPa, respectively. A reduction of the angle by about 0.6° occurs for the same applied pressure (16.28 GPa) within the LSDA. We thereby establish that, regardless of the kind of DFT one is using, on applying pressure ∠Mn-O-Mn does not increase but rather decreases, though almost insignificantly. The major effects comes from a reduction in the bond lengths. In the following calculations, we have therefore kept the ∠Mn-O-Mn unchanged upon application of pressure.

We have carried out LSDA total energy calculations for various spin arrangements of Mn atoms as explained in Sec. II. The relative LSDA total energies, as given in Table III, are mapped onto Eq. (1) in order to extract the J's. The magnetic exchange interaction strengths are calculated and shown in Table IV for an almost 2% reduction in experimental lattice parameter, amounting to a pressure of 16.28 GPa. Considering a pressure of 16.28 GPa, we observe a substantial decrease in the NN FM interaction. The 2NN and 3 NN interactions remain almost the same. This leads to a mean-field T_c of about 140 K, leading to a decrease of about 41 K. The gradient is about −2.5 K/GPa. The gradient calculated from another set of calculations at 3.04 GPa is about −2.3 K/GPa. One can approximate a linear relation between T_c and applied pressure. Thus the average gradient is about −2.4 K/GPa. This is not an unreasonable estimate considering the mean-field overestimation. The ratio of exact T_c and T_c^{mf} is estimated as 0.79 and 0.81 for bcc and fcc lattices with coordination 8 and 12, respectively. Considering the average coordination of 10 for Mn sublattice in $Tl_2Mn_2O_7$, one would expect the gradient in T_c to be about −1.9 K/GPa. This is a bit larger than the experimental values, which are −1.6 K/GPa (Ref. 6) and about −1 K/GPa (Ref. 15). A plausible explanation for this somewhat overestimation may be due to computational limitations imposed by the number of spin configurations. A better estimate of the gradient might have been reached had all the possible spin configurations been considered for calculation of the J's. Therefore one can conclude that within the limitation of our method, we have established the trend in ferromagnetism of $Tl_2Mn_2O_7$ with applied pressure correctly.

In Fig. 6 we show the density of states of $Tl_2Mn_2O_7$ under 16.28 GPa pressure along with that of $Tl_2Mn_2O_7$ under ambient pressure for comparison. Upon application of pressure, the bond lengths shorten, which enhances the Mn-O and

TABLE III. Relative LSDA energies per Mn ion in meV in FM and five AFM spin configurations for $Tl_2Mn_2O_7$ at normal, 3.04 GPa, and 16.28 GPa pressures. All energies are converged up to 0.01 meV per Mn ion.

	ΔE (meV)		
	Normal	3.04 GPa	16.28 GPa
FM	0	0	0
AFM1	9.55	9.18	7.36
AFM2	13.98	14.17	13.05
AFM3	12.24	11.49	8.82
AFM4	17.59	22.5	16.24
AFM5	18.39	17.7	14.04

TABLE IV. NN, 2NN, 3NN, and effective exchange interaction strengths and mean-field Curie temperature calculated within the LSDA at ambient condition and at 3.04 and 16.28 GPa for $Tl_2Mn_2O_7$.

Pressure appl. (GPa)	J_1 (meV)	J_2 (meV)	J_3 (meV)	J_0 (meV)	T_c^{mf} (K)
0	−2.52	−0.11	+0.33	12.48	181
3.04	−2.48	−0.16	+0.40	12.06	174
16.28	−1.99	−0.16	+0.35	9.66	140

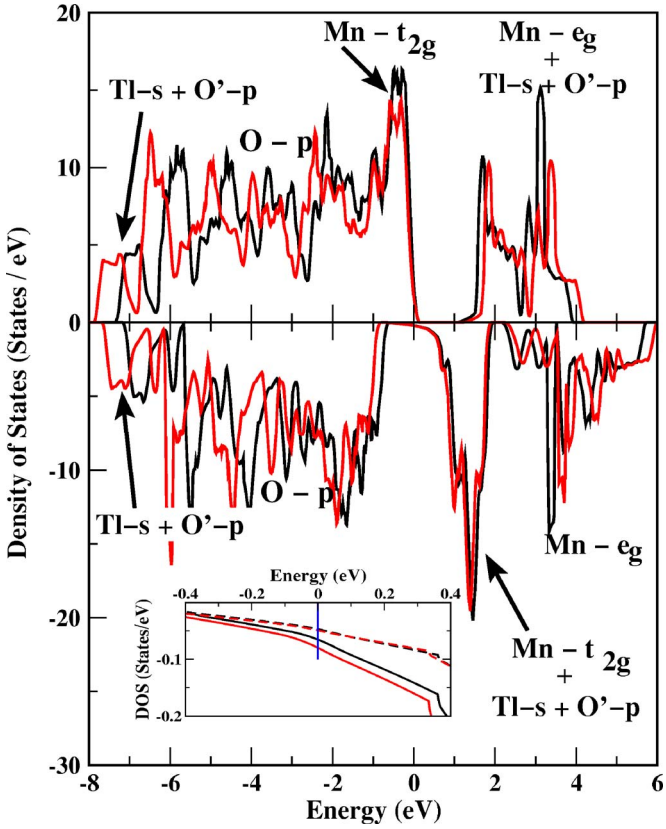

FIG. 6. (Color online) Spin-polarized density of states at ambient condition (black) and 16.28 GPa (red) calculated within the LSDA for $Tl_2Mn_2O_7$. The upper (lower) panel corresponds to the majority (minority) spin. The negative of the density of states has been plotted in the lower panel for clarity. The inset shows the minority-spin channel density of states for the energy region near the Fermi level at ambient and 16.28 GPa. The solid and dashed lines show the contribution from Mn $3d$ and Tl$-6s+$O$'-2p$ states, respectively, within the LSDA.

Tl-O′ interaction, and as a result the net bandwidth expands and the t_{2g}-e_g splitting is enhanced. However, the key effect is seen in the inset, where we show the Mn d– and Tl s–projected density of states in an energy window close to E_F as solid and dashed lines, respectively. They are shown in two different colors, corresponding to ambient and 16.28 GPa pressure. We notice that the relative proportion of Tl-O′ in the hybridized, dispersive band has reduced significantly upon application of pressure. It has reduced from 45% in the case of ambient pressure to 36% in the case of 16.28 GPa pressure. This indicates a reduction of Mn-Tl-O′ hybridization upon application of pressure. Since the underlying mechanism of ferromagnetism is based on the Mn-Tl-O′ hybridization, weakening of such a hybridization would cause a decrease in T_c as supported by the detailed calculation presented above. The change in the hybridization is proportional to the change in the hopping interaction strength t and inversely to the change in the energy level separation Δ. Application of pressure causes a shortening of the bond length; hence, one would expect hopping to increase and in turn the hybridization to increase, opposite to what is observed in the calculation. For this we performed

TABLE V. Relative LSDA energies per Mn ion in meV in FM and five AFM spin configurations for doped $Tl_2Mn_2O_7$. All energies are converged up to 0.01 meV per Mn ion.

	ΔE (meV)		
	$x=0$	$x=0.125$	$x=0.25$
FM	0	0	0
AFM1	9.55	16.50	23.96
AFM2	13.98	26.07	29.39
AFM3	12.24	23.18	31.53
AFM4	17.59	33.30	35.69
AFM5	18.39	34.39	40.11

the NMTO-downfolding calculation keeping Mn $3d$, Tl $6s$ and O $2p$ degrees of freedom active and integrating out the rest, including O′ degrees of freedom to define a Tl-O′ effective level. The real-space representation of that downfolded Hamiltonian in the NMTO-Wannier function basis for $Tl_2Mn_2O_7$ under application of 16.28 GPa pressure shows the Tl-O′ effective level to shift down by 0.3 eV compared to that under ambient pressure. This increases the Δ and substantially reduces the Tl-O′-Mn hybridization, substantial enough to compensate for the increase in $t_{sd\sigma}$ hopping interaction between Mn t_{2g} and the effective Tl s orbital and to, produce a net negative contribution to the hybridization. This is an interesting, counterintuitive situation which can only be unraveled by a detailed analysis of the underlying electronic structure as has been done in the present study.

C. Sb-doped $Tl_2Mn_2O_7$

To mimic the doping effect, we have carried out calculations using supercell containing 16 Mn atoms. The construction of such supercell has been described in Sec. II. Out of these 16 Mn atoms, some are substituted by Sb to simulate the effect of doping. There are two doping levels that have been investigated. In one case, one of the Mn atom is substituted by an Sb atom, and in another case, two of the Mn atoms are replaced by two Sb atoms. The former amounts to doping level of $x=0.125$ or 6.25% and the latter amounts to doping of $x=0.25$ or 12.5%. These are not exactly the doping levels that hav been investigated experimentally but close to them (i.e., $x=0.1$ and 0.2, respectively).

Substitution of Mn^{4+} by a larger cation Sb^{5+} does not cause any significant changes in the crystal structure other than the fact that the lattice expands slightly, keeping the various angles unchanged. The lattice parameters corresponding to doping levels of $x=0.125$ and 0.25 are obtained by interpolation of the experimentally determined lattice constants at various doping as shown in the inset of Fig. 1 in Ref. 8. The lattice parameters for $x=0.125$ and 0.25 are increased by 0.3%, and 0.9%, respectively, compared to the undoped lattice constant.

To estimate the exchange interaction strengths for $Tl_2Mn_{2-x}Sb_xO_7$ with $x=0.125$ and 0.25 we have carried out LSDA total energy calculations for various spin arrangements of Mn atoms as explained in Sec. II. The relative

TABLE VI. Exchange interaction strengths J_1 (NN), J_2 (2NN), and J_3 (3NN) and effective exchange coupling strength J_0 in meV, total density of states at Fermi level, $D(E_F)$, and mean-field Curie temperature T_c^{mf} for $Tl_2Mn_{2-x}Sb_xO_7$, x=0.0, 0.125, and 0.25.

Doping conc.	J_1 (meV)	J_2 (meV)	J_3 (meV)	J_0 (meV)	$D(E_F)$ (states/eV)	T_c^{mf} (K)
x=0.0	−2.52	−0.11	+0.33	−12.48	0.2	181
x=0.125	−3.65	−0.12	−0.41	−26.38	1.0	382
x=0.25 (3NN)	−2.72	−0.57	−0.85	−29.08	1.4	422
x=0.25 (NN)	−2.74	−0.56	−0.87	−29.30	1.44	423

LSDA total energies, as given in Table V, are mapped on to Eq. (1) in order to extract the J's. At 6.25% doping the average coordination numbers change to 5.6, 11.2, and 11.2, respectively. In order to check whether the chosen disordered configuration has any influence on the trend, we have repeated the calculation with two Sb atoms in the unit cell for two cases. In one case, two Sb atoms were chosen as NN pairs while in the second case they have been chosen as 3NN pairs. The respective coordination numbers at 12.5% doping are 5.14, 10.28, and 10.86 for 3NN substitution and 5.28, 10.28, and 10.28 for NN substitution. In all the three cases–i.e., for x=0.125, 0.25 (NN), and 0.25 (3NN)—the ground state is found to be FM.

Table VI gives the magnetic exchange interaction strengths for all the three cases and their corresponding T_c's and density of states at E_F, $D(E_F)$. For comparison, we also quote the numbers corresponding to pure $Tl_2Mn_2O_7$ taken from Ref. 9. Pristine $Tl_2Mn_2O_7$ has a very strong NN FM interaction, a weak 2NN FM interaction, and a little stronger 3NN AFM interaction. With the introduction of doping, all the interactions became FM and their strengths also increase. On further increase of doping, the 2NN and 3NN FM interactions become stronger with a small decrease in the NN FM interaction. It is worth mentioning here that the result for x =0.25 doping with two NN Mn atoms substituted does not change significantly compared to the result when the two Mn ions substituted were 3NN's, proving that the choice of disordered configuration does not alter the general trend. Computation of T_c, using the values of J_1, J_2, and J_3, listed in Table I, show a rapid increase in T_c on the initial doping which then attains a kind of saturation on further doping, considering up to a moderate level of doping. This trend is in good agreement with experimental findings, but the quantitative values differ. This happens primarily because of the clustering effect not included in our calculation. To quote Alonso *et al.*,[8] "For low doping levels, we cannot disregard some type of magnetic clustering with almost pure $Tl_2Mn_2O_7$ (T_c=135 K) and Sb-rich regions." Such effects are bound to reduce the global T_c measured experimentally. Also lattice relaxation effect could be important. Although experimentally measured crystal structure data show the same space group symmetry as those of the undoped one with little variation in the internal u parameter, the substitution of the Mn ion by a larger cation will probably change the structure locally. Therefore structural relaxation of the doped compounds, which is beyond the scope of our present computational capacity, are needed to resolve the issue completely.

One needs to examine the electronic structure upon doping to understand the microscopic origin of the striking effect described above. In Fig. 7 we show the density of states corresponding to Sb-doped $Tl_2Mn_2O_7$ for doping levels of x=0.125 and 0.25. To appreciate the changes in the electronic structure upon doping, we also show the density of states for pure $Tl_2Mn_2O_7$. Comparing the various density of states, we observe a slight shrinking of the overall bandwidth due to the small expansion of the lattice. The t_{2g}-e_g splitting at the Mn site decreases due to expansion of the Mn-O bond length. Smearing of the DOS, compared to pure case, is also

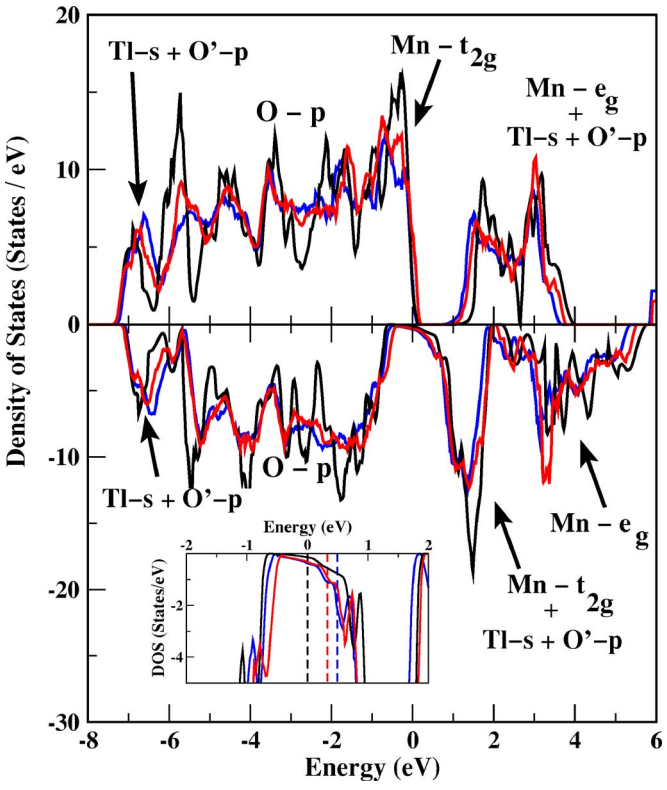

FIG. 7. (Color online) Spin-decomposed density of states for x =0.0 (black), 0.125 (red), and 0.25 (blue) doping in $Tl_2Mn_{2-x}Sb_xO_7$. Zero of the energy is set at the Fermi level of the undoped $Tl_2Mn_2O_7$ compound. The upper (lower) panel corresponds to the majority (minority) spin. The negative of density of states has been plotted in the lower panel for clarity. The inset shows the density of states in the minority-spin channel at the same doping levels for the energy region close to the Fermi level. The dashed lines in the inset correspond to the respective Fermi levels.

observed due to the effect of disordering. The Sb ions in the 5+ state have completely filled 4*d* shells which are essentially core like while 5*s* and 5*p* states remain more or less empty with no contribution to the states close to E_F. The most important effect is that of electron doping. Replacement of Mn^{4+} by Sb^{5+} introduces additional electrons in the system which have no other option but to populate the highly dispersive Tl-O′-Mn t_{2g} hybrid state in the minority-spin channel. Because of the highly dispersive nature of this band, the density of state in the minority-spin channel close to E_F rises fast after the tail part which then attains a kind of small plateau before attaining highly peaked values corresponding to weakly dispersive Mn t_{2g} dominated states between 1 and 2 eV. This is shown in the inset of Fig. 7. With the introduction of a first Sb atom, the doped extra electrons while populating the dispersive minority-spin band increase $D(E_F)$ substantially. Upon increasing the number of Sb atoms from 1 to 2, the Fermi level shifts towards the right to accommodate more electrons, but since it has almost crossed the highly dispersive region and falls within the plateaulike structure, $D(E_F)$) does not change significantly. This is evident by quantitative estimates of $D(E_F)$ shown in Table I. In Fig. 7, we have shown only the case of $x=0.25$ (NN), but the DOS corresponding to $x=0.25$ (3NN) is not very different and $D(E_F)$ changes only marginally. Following the perturbative treatment in terms of the transfer integral,[27] t between the magnetic and nonmagnetic site, the exchange coupling J within the proposed kinetic-energy-driven scheme is given by $t^4D(E_F)/\Delta^2$, where Δ is the average energy separation between the magnetic and nonmagnetic levels and $D(E_F)$ is the density of states at Fermi level introduced in the above. The real space representation of the NMTO-downfolded Hamiltonian keeping Tl 6*s*, Mn 3*d*, and O 2*p* states active and downfolding the rest shows that the Tl-Mn hopping integral t's and their energy level separation change only slightly for 0.3% and 0.9% expansion of the lattice upon $x=0.125$ and 0.25 doping. The major changes come from the sharp increase in $D(E_F)$ which explains the enhancement of J's and T_c's in turn.

IV. CONCLUSIONS

We have presented a detailed study of $Tl_2Mn_2O_7$ under pressure and Sb-doped $Tl_2Mn_2O_7$ using first-principles electronic structure calculations. The analysis of the computed electronic structure shows that the counterintuitive experimental observation of the suppression of ferromagnetic T_c upon application of pressure and its enhancement upon moderate amount of doping by Sb in Mn sublattices is naturally explained in terms of the hybridization-induced mechanism proposed earlier.[9] Application of pressure reduces the hybridization between the localized Mn t_{2g} level and the delocalized Tl-O′ effective state due to the shifting of the position of the Tl-O′ effective level, which weakens the driving mechanism of ferromagnetism and thereby reduces the strength of exchange coupling and the T_c.

In case of doping, on the other hand, the enhancement of T_c is induced by the charge-carrier doping of the system by Sb. This enhances the value of the density of states at the Fermi energy significantly, thereby enhancing the exchange coupling and the T_c. Our conclusions were substantiated by the explicit calculation of the J's and T_c's.

In the case of $Tl_2Mn_2O_7$ under pressure, we resolved the issue related to the change in Mn-O-Mn angle. We carried out structural relaxation by means of accurate pseudopotential-based total energy calculations. Our theoretical results show, as opposed to the claim by Velasco *et al.*,[15] that the Mn-O-Mn angle decreases, in agreement with the original suggestion by Sushko *et al.*[6] However the decrease is only marginal, and for all practical purposes, it may be assumed to remain same as that of $Tl_2Mn_2O_7$ in ambient condition. This rules out the use of an angle variation argument to explain the reduction of T_c.

ACKNOWLEDGMENTS

The research was funded by DST Project No. SR/S2/CMP-42/2003. We thank the MPG-partnergroup program for the collaboration.

*Also at Jawaharlal Nehru Center for Advanced Scientific Research and Center for Condensed Matter Theory, IISc, Bangalore, India.

[1] H. Y. Hwang and S.-W. Cheong, Nature (London) **389**, 942 (1997).
[2] Y. Shimakawa, Y. Kubo, and T. Manako, Nature (London) **379**, 53 (1996).
[3] H. Okamura, T. Koretsume, M. Matsunami, S. Kimura, T. Nanba, H. Imai, Y. Shimakawa, and Y. Kubo, Phys. Rev. B **64**, 180409(R) (2001).
[4] J. Sanchez-Benitz, A. de Andres, C. Prieto, J. Avila, L. Martin-Carron, J. L. Martinez, J. A. Alonso, M. J. Martinez-Lope, and M. T. Casais, Appl. Phys. Lett. **84**, 4209 (2004).
[5] A. Ramirez and M. A. Subramanian, Science **277**, 546 (1997).
[6] Yu. V. Sushko, Y. Kubo, Y. Shimakawa, and T. Manako, Physica B **259-261**, 831 (1999).
[7] J. A. Alonso, M. J. Martínez-Lope, M. T. Casais, P. Velasco, J. L. Martínez, M. T. Fernandez-Díaz, and J. M. de Paoli, Phys. Rev. B **60**, R15024 (1999).
[8] O. K. Andersen and T. Saha-Dasgupta, Phys. Rev. B **62**, R16219 (2000); O. K. Andersen, T. Saha-Dasgupta, and S. Ezhov, Bull. Mater. Sci. **26**, 19 (2003) and references therein.
[9] T. Saha-Dasgupta, M. De Raychaudhury, and D. D. Sarma, Phys. Rev. Lett. **96**, 087205 (2006).
[10] M. D. Núñez-Regueiro and C. Lacroix, Phys. Rev. B **63**, 014417 (2000).
[11] D. D. Sarma, Priya Mahadevan, T. Saha-Dasgupta, Sugata Ray, and Ashwani Kumar, Phys. Rev. Lett. **85**, 2549 (2000).
[12] D. D. Sarma, Curr. Opin. Solid State Mater. Sci. **5**, 261 (2001).
[13] P. Mahadevan, A. Zunger, and D. D. Sarma, Phys. Rev. Lett. **93**, 177201 (2004).

[14] Y. Shimakawa (private communication). Mn-O-Mn decreases in the small experimental pressure range.
[15] P. Velasco, J. A. Alonso, V. G. Tissen, W. G. Marshall, M. T. Casais, M. J. Martínez-Lope, A. de Andres, C. Prieto, and J. L. Martínez, Phys. Rev. B **67**, 104403 (2003).
[16] O. K. Andersen and O. Jepsen, Phys. Rev. Lett. **53**, 2571 (1984).
[17] N. M. Rosengaard and B. Johansson, Phys. Rev. B **55**, 14975 (1997).
[18] X. Wan, M. Kohno, and X. Hu, Phys. Rev. Lett. **94**, 087205 (2005).
[19] M. A. Subramanian, B. H. Toby, A. P. Ramirez, W. J. Marshall, A. W. Sleight, and G. H. Kwei, Science **273**, 81 (1996).
[20] D. Vanderbilt, Phys. Rev. B **41**, R7892 (1990).
[21] G. Kresse and J. Hafner, Phys. Rev. B **47**, 558 (1993); G. Kresse and D. Furthmüller, Comput. Mater. Sci. **6**, 15 (1996); Phys. Rev. B **54**, 11169 (1996).
[22] P. E. Blöchl, Phys. Rev. B **50**, 17953 (1994); G. Kresse and D. Joubert, *ibid.* **59**, 1758 (1999).
[23] F. D. Murnaghan, Proc. Natl. Acad. Sci. U.S.A. **30**, 244 (1944).
[24] The importance of Tl-O-Mn hybridization has also been indicated earlier by C. I. Ventura and B. Alascio [Phys. Rev. B **56**, 14533 (1997)] and by Y. Shimakawa, Y. Kubo, N. Hamada, J. D. Jorgensen, Z. Hu, S. Short, M. Nohara, and H. Takagi [Phys. Rev. B **59**, 1249 (1999)].
[25] M. De Raychaudhury, T. Saha-Dasgupta, and D. D. Sarma (unpublished).
[26] C. J. Fennie and K. M. Rabe, Phys. Rev. B **72**, 214123 (2005).
[27] J. Kanamori and K. Terakura, J. Phys. Soc. Jpn. **70**, 1433 (2001).